RSC Advances

PAPER

View Article Online
View Journal | View Issue

Cite this: *RSC Adv.*, 2020, **10**, 2877

Microscopic investigations on the healing and softening of damaged salt by uniaxial deformation from CT, SEM and NMR: effect of fluids (brine and oil)

Jie Chen,† Huihua Peng, †* Jinyang Fan, Xiong Zhang, Wei Liu and Deyi Jiang*

Nowadays, a salt cavern, used as underground energy storage (*e.g.* natural gas, crude oil, hydrogen), is becoming more and more popular in China due to its many advantages, such as low permeability ($\leq 10^{-21}$ m^2), good water-soluble mining and the damage-healing characteristic of salt rocks. It not only solves the problem of energy resource supply-demand imbalance in China, but also provides a better, more secure and cost-effective way to store energy compared to aboveground energy storage systems. As for salt cavern storage, permeability is our primary concern in engineering, which is mainly influenced by damage and healing. In this work, some damaged salt specimens were prepared by uniaxial compression tests (the loading rate was 0.033 mm s^{-1}). Then those specimens were immersed in either a saturated brine solution or oil at 50 °C for a few days. Microscopic investigations were carried out by X-ray Computed Tomography (CT), Scanning Electron Microscope (SEM) and Nuclear Magnetic Resonance (NMR) to investigate the change of salt microstructures after healing. Possible micro-healing mechanisms were discussed. It was found that fluids played an important role in the healing process of damaged salt. Healing effectiveness of micro-pores and -cracks with the brine solution was higher than that with oil mainly because of crystal recrystallization. The surface of the grains was smooth and had no visible microcracks after healing in brine, while there were many pits and micro-tunnels with oil. Oil could hinder the healing process by impeding the diffusion effect and restraining grain recrystallization. Meanwhile, intragranular and intergranular water could also work as a lubricant resulting in softening which made salt rock more deformable. NMR results confirmed that damaged salt had a better recovery with brine, displaying lower porosity and lower permeability compared to that with oil. This work provides preliminary microscopic investigations on the healing of damaged salt in order to reveal the salt healing mechanism.

Received 29th July 2019
Accepted 6th January 2020

DOI: 10.1039/c9ra05866d

rsc.li/rsc-advances

1. Introduction

What is the power source of modern industrial development? What is the indispensable strategic resource for the survival and development of a country? And what kind of resource plays an inestimable role in safeguarding the national economy, social development and national defense security? The 'black gold'-petroleum![1,2] As a strategic plan, the Strategic Petroleum Reserve (SPR) project has been very popular in developed countries after the first oil crisis in 1973. A safe standard of SPR for a country is 90 days declared by the International Energy Agency (IEA). By 2016, the USA had already reached the SPR's demand of 150 days as well as Japan's SPR. What's more, Germany's SPR was 120 days.[3] However, China's SPR is far behind these developed countries at present.[4] To solve this problem, China's SPR has been scheduled to be constructed between 2003 and 2020 and is divided into three phases. Most of the reserve bases are located in coastal cities, such as Dalian, Huangdao, Zhoushan and Zhenhai (Fig. 1). When it is completed in 2020, China's petroleum reserve capacity will increase to about 85 million cubic metres, equivalent to 90 days of net oil imports. Nowadays, China's SPR phase III is still underway. Salt caverns are considered to be the most ideal site for SPR due to the following advantages:[5–8]

(1) Good tightness. Rocksalt is well known as a kind of very low permeability ($<10^{-20}$ m^2) and low porosity (<1%) material.[9–11]

(2) High security. Salt caverns are usually located at a depth of hundred meters to thousand meters underground, which is not easily affected by man-made destruction or natural disasters aboveground.[12,13]

School of Resources and Safety Engineering, State Key Laboratory of Coal Mine Disaster Dynamics and Control, Chongqing University, Chongqing 400044, PR China. E-mail: huihuapeng@cqu.edu.cn; deyij@cqu.edu.cn

† These authors contributed equally to this work.

Fig. 1 Distributions of SPR bases and main salt mines in China. Jintan, Huai'an and Yingcheng salt mines are considered to be the most potential sites for SPR phase III.

(3) Environmental friendly. The floor area of salt caverns on the surface is usually small without potential oil leakage aboveground.

(4) Large storage. Each single salt cavern has a storable volume of (10–100) $\times$ 10^4 m^3. Typically, only about thirty salt caverns are needed to store 1000 $\times$ 10^4 m^3 of petroleum.

(5) Easy injection-withdrawal.

(6) Good economic benefit. For instance, a barrel of crude oil in the Gulf of Mexico when stored in salt caverns costs only \$1.5.

Due to these advantages, many developed countries have used salt caverns as the SPR base. In the USA, for example, almost all of strategic oil reserves are located in underground salt caverns. China has widespread salt formations,[14,15] like Jintan, Huai'an and Yingcheng salt mines (Fig. 1), which have been proved to be feasible for SPR.[4,10] The expected petroleum reserve is about 30 million cubic meters, which can completely meet the Chinese SPR's goal (Fig. 2).

Regarding a salt cavern, no oil leakage is the most important criteria. Therefore, permeability is the primary concern in engineering and is mainly influenced by salt damage and healing.[16,17] In the last few decades, damaged salt healing mechanism and many influencing factors, such as confining stress, temperature, water, fracture morphology and impurities, have been widely researched.[18,19] A suitable quantity of water and level of temperature can promote crack healing.[19,20] Inclusions or impurities can significantly reduce the healing effectiveness.[18,21] Healing of fluid-filled grain boundaries or microcracks is very common in natural wet salt at sufficiently low intergranular effective stress due to the low activation energy for recovery.[20] Studies confirm that healing processes are governed by mechanical closure, compaction creep, and interfacial-energy-driven processes like pressure solution and recrystallization.[22–25] Meanwhile the healing process can inhibit pressure solution (progressive reduction of the contact area filled by connected fluid).[26] However, the damage-healing model is still hard to build because of not precisely clear mechanism.[27,28] The key solution is to study it from microscopic scale.[24,29,30] In addition, it can be said that the effect of healing has not been well applied in engineering practice, especially for oil storage. Further work is still needed in this area. In this contribution, damaged salt's healing as well as softening were investigated from a microscopic scale using CT, SEM and NMR. Effects of fluids (brine and oil) and mechanism were analyzed and discussed.

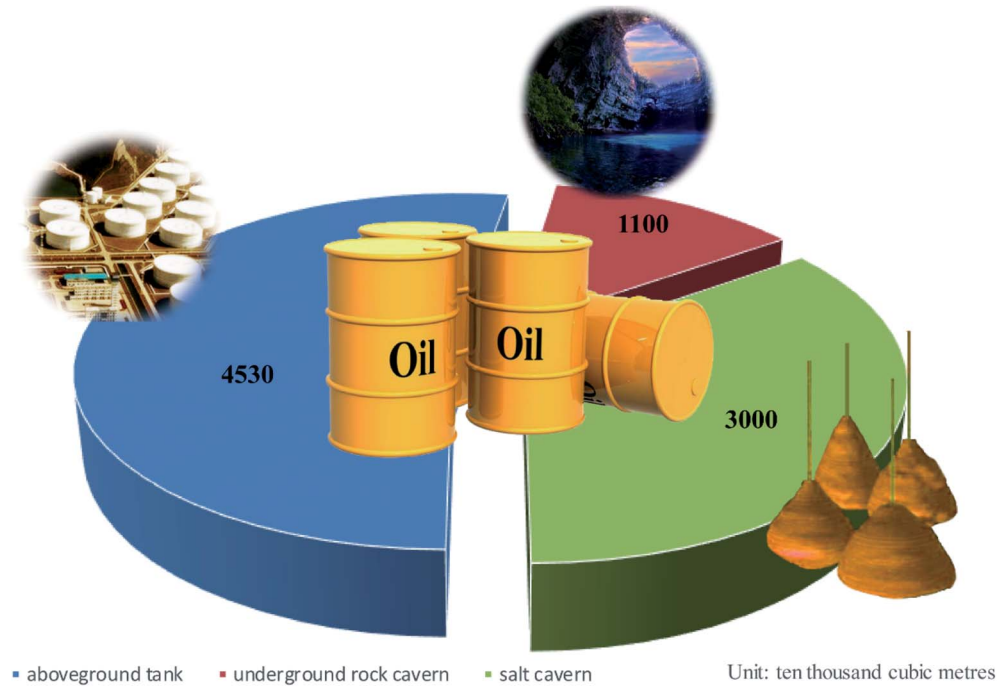

Fig. 2 Distribution of expected oil reserves in aboveground tank, underground rock cavern and salt cavern for China SPR project. Total oil reserve is expected to 86.3 million cubic metres, which can fully meet the SPR's goal (85 million cubic metres by 2020, equivalent to 5.4×10^8 barrels).

2. Experimental section

2.1 Materials

In the present paper, several salt samples collected from the Khewra salt mine in Pakistan were prepared. These salt samples were mainly composed of sodium chloride (higher than 96%) and small amounts of potassium sulfite.[31] Samples were dry cut and polished into standard cylindrical blocks of 100 mm length and 50 mm diameter according to the International Society of Rock Mechanics (ISRM) testing standard.[32] Before testing, all samples were wrapped in polyethylene plastic films and stored in a dry oven.[33] Saturation brine solution was prepared by dissolving rocksalt powder in a deionized water at 50 °C. L-HM68 hydraulic oil purchased from Sinopec Group was used here.

2.2 Damage and healing methods

Damaged salt specimens were prepared by uniaxial compression tests using a conventional rock mechanics testing machine (RMTM, Fig. 1a), which was independently developed and manufactured by the state key laboratory of coal mine disaster dynamics and controls. Specimens were damaged until the loading stress approximately reached 25 MPa, which accounted for about (50–60)% of the rocksalt strength.[34] The loading rate was 0.033 mm s^{-1}. After damage, the samples were immersed in a saturated brine solution or oil at 50 °C for seven days. For comparisons, these samples were again loaded by the uniaxial compression tests until failure. What's more, a set of comparative experiments were also tested without undergoing the healing process. Sample numbers and the experimental schedule are displayed in Table 1.

2.3 Characterizations

CT. CT imaging is a good way of non-destructive investigation to detect the internal damage of rocksalt.[35] All CT tests were executed by a CT experimental system purchased from Siemens Shanghai co. LTD (SOMATOM Scope, Fig. 3b), which could be coupled with heat, fluid and solid. The interval of CT images was 0.6 mm. Samples were scanned by the CT machine before/after damage and after healing. Post-processing of CT images undertaken using Matlab and ImageJ.

SEM. The morphological information and microstructures of as-prepared original salt, damaged salt and healed salt samples were characterized by Scanning Electron Microscopy (Zeiss Auriga SEM, Fig. 3c). The resolution of SEM equipped with EDS detector and EBSD can be up to 10 nm (15 kV). Specimens were gold coated before imaging to prevent charging effects.[36]

NMR. Porosity and pore size distribution of rock cores were assessed using a non-destructive NMR system from Suzhou Niumag Analytical Instrument Corporation (MacroMR12-150H-I, Fig. 3d). The system is composed of four main parts, including an NMR analyzer, an MRI system, a high temperature–high pressure probe and other accessories. Rock cores with 60 mm diameter and 120 mm length are the largest sizes that can be tested. Magnetic field intensity is 0.3 ± 0.05 T. Pore size ranging from few nanometers to hundred micrometers can be detected. Preliminary permeability of specimens can also be predicted by NMR.

Table 1 Experimental schedule and corresponding damage and recovery rate[a]

Samples No.	Initial deformation	Healing conditions	Healing time/d	Initial damage/%	Residual damage/%	Recovery rate/%#
A2-50-1*	Uniaxial compression: σ_1 is up to 25 MPa (about (50–60%) σ_{max}); loading rate: 2 mm min^{-1}.	Saturated brine solution: 50 °C	7	1.57	0.84	46.23
A2-50-2*		Oil bath: 50 °C	7	1.69	1.07	36.61
A2-50-3		—	0	1.59	—	0
A-50-3*		—	0	—	—	0

[a] σ_{max} is rocksalt uniaxial strength, σ_1 is maximum loading stress. # Recovery rate = (initial damage − residual damage)/initial damage × 100%, calculated from a series of resulting CT images; *the three test sequences include second deformation test in comparison with the first one.

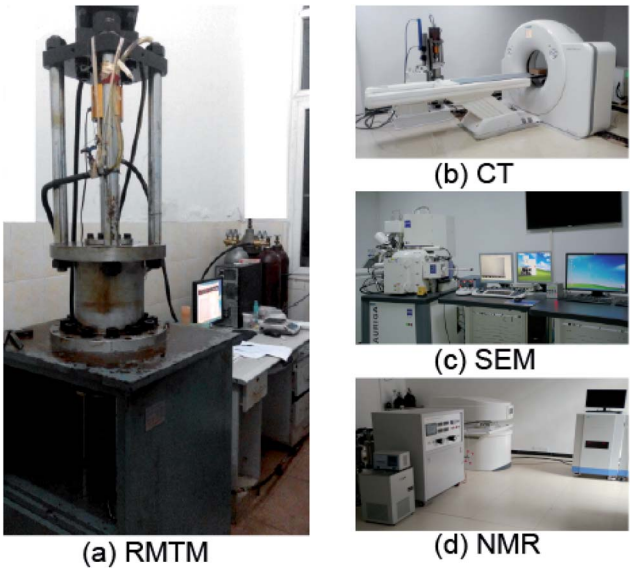

Fig. 3 Digital photos of experimental equipment.

3. Results and discussion

3.1 Salt mechanical properties

Typical stress–strain (σ–ε) curves of salt samples are shown in Fig. 4. Digital photo of healed salt samples revealed that the cylindrical salt samples were not dissolved but kept in good shape. Oil particles could penetrate inside the damaged salt (Fig. 4a). Fig. 4b shows the σ–ε curves of the first test (initial damage). All samples were damaged by uniaxial compression test until the maximum principal stress (σ_1) was up to 25 MPa (loading force, F, was about 50 KN). Because of the discreteness of rock samples, axial strains ranged from 2% to 2.75%. Damage points were located in the plastic zone. Generally, all σ–ε curves of the initial damage displayed a similar behavior. However, the σ–ε curves of the second test after salt healing exhibited a different behavior, as shown in Fig. 4c. Healed salt samples with brine solution were more ductile than samples without fluid. For the sake of contrast, the σ–ε curves between the first and the second test were individually drawn in a graph (Fig. 4d–f). As shown in Fig. 4f, rock salt without fluid displayed an obvious strain hardening during the second press due to the dislocations.[37] Rock salt with fluid (oil, Fig. 4e), however, became less hardening during the second press. With the influence of water (brine, Fig. 4d), rock salt tended to softening or weakening.[38] Intragranular and intergranular water could also work as lubricant resulting in material's softening which made salt rock more deformable. Strength and Young's modulus were calculated at a strain of 0.01 for both the first and the second press (Table 2). The change rate of Young's modulus verified the results of strain hardening and water weakening. Herein, strain hardening is defined that the resistance to deformation of rock salt is enhanced after the yield stage, as the dislocation propagation is hindered. On the contrary, weakening is defined as the reduction of the deformation resistance.

3.2 CT

Fig. 5 displays the schematic diagram of CT scanning sections and the resultant CT grayscale images of the original rock salt (A0). The corresponding gray histograms from the horizontal (H1) and vertical (V1) sections in the middle position of specimen both showed one major peak, which indicates that original specimens have negligible damage. The non-destructive investigation on the internal damage of rock salt was performed with CT imaging. Typical CT images are displayed in Fig. 6. 3D views of rock samples were reconstructed from a series of CT slices with an interval of 0.6 mm, which visually showed the initial damage (A1 and B1) after the first press and the residual damage (A2 and B2) after healing. It was clearly observed from the cross sections that the internal damage of rocksalt decreased after healing. Then CT slices were binarized in order to quantitatively calculate the initial and residual damage. Computed results are shown in Table 1. It was found that the initial damage of all salt specimens was almost the same thus verifying that the approach was reliable. Healing effectiveness was calculated by the following eqn (1)

$$\text{Recovery rate} = \frac{\text{initial damage} - \text{residual damage}}{\text{initial damage}} \times 100\% \quad (1)$$

Results showed that the healing effectiveness with the brine aqueous solution was much higher than that with oil, indicating that water played an important role in the healing of damaged salt mainly because of crystal recrystallization. Nevertheless, oil could hinder the healing process by impeding the diffusion effect or restraining grain recrystallization.

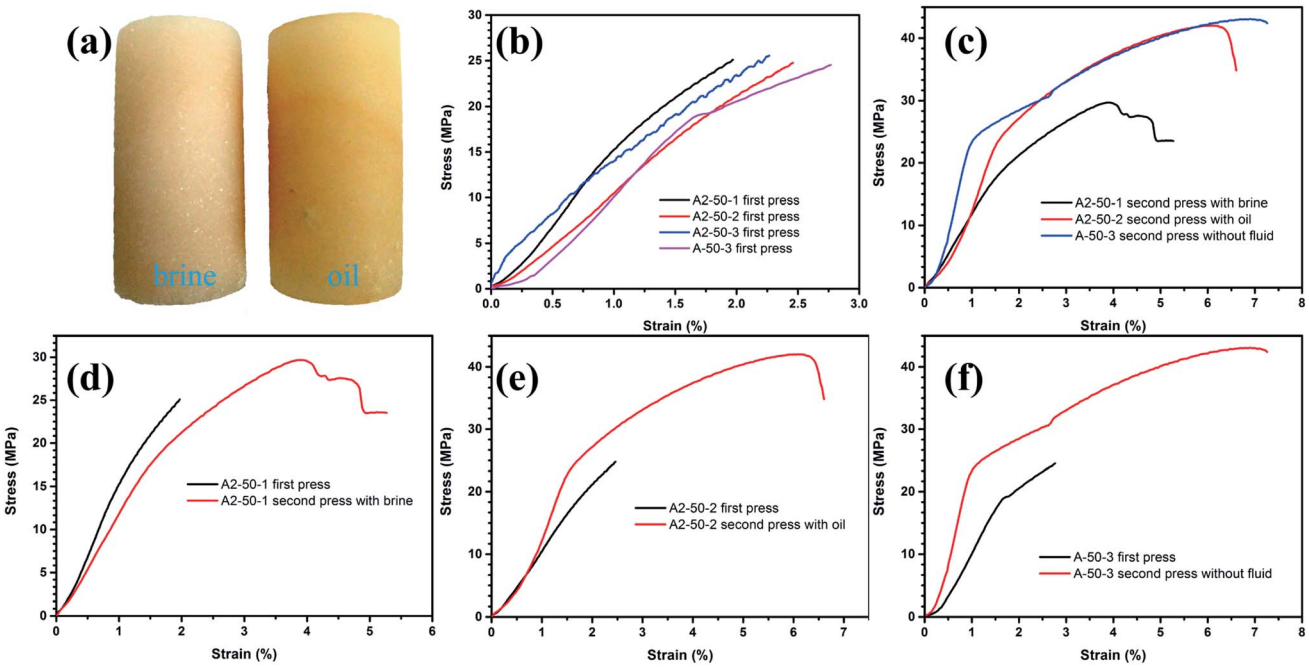

Fig. 4 (a) Photograph of cylindrical salt samples after immersed in saturated brine and oil for 7 days. Stress–strain curves of (b) first test (initial damage), (c) second test, and (d–f) comparisons between both tests.

Table 2 Strength and Young's modulus calculated at strain of 0.01 in the first and second uniaxial deformation, and the change rate of elastic modulus

	First test		Second test		
Samples no.	σ_1/MPa	E_1/GPa	σ_2/MPa	E_2/GPa	$(E_2 - E_1)/E_1 \times 100\%$
A2-50-1	15.25	1.52	11.79	1.18	−22.55
A2-50-2	10.46	1.04	12.49	1.23	17.46
A-50-3	10.35	1.02	23.63	2.31	127.92

3.3 SEM

To uncover the potential healing mechanism of rocksalt and the effect of fluids (brine and oil), some representative salt samples were selected for SEM (Fig. 7). As shown in Fig. 7a, original rocksalt consisted of intact coarse cube-shaped grains without obvious cracks or voids. The surface of grains was smooth. However, coarse grains were transformed into irregularly shaped grains with many angular fragments after the initial damage, showing abundant inter-/intra-granular fractures, microcracks and multiple shear cracks (highlighted in Fig. 7b).

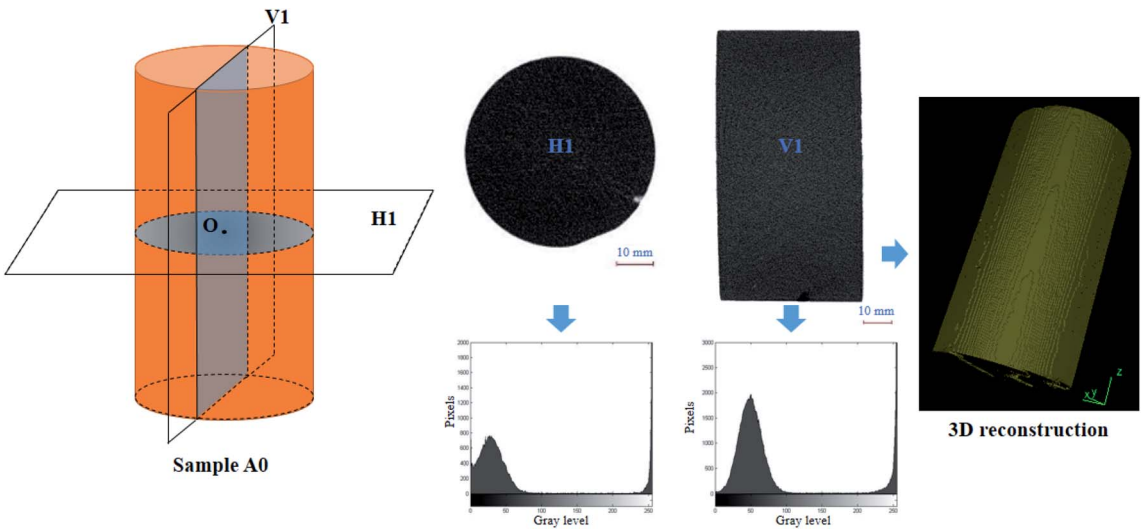

Fig. 5 Schematic diagram of CT scanning sections and the resultant CT grayscale images of original salt (sample A0). The corresponding gray histograms and 3D reconstruction model are also given.

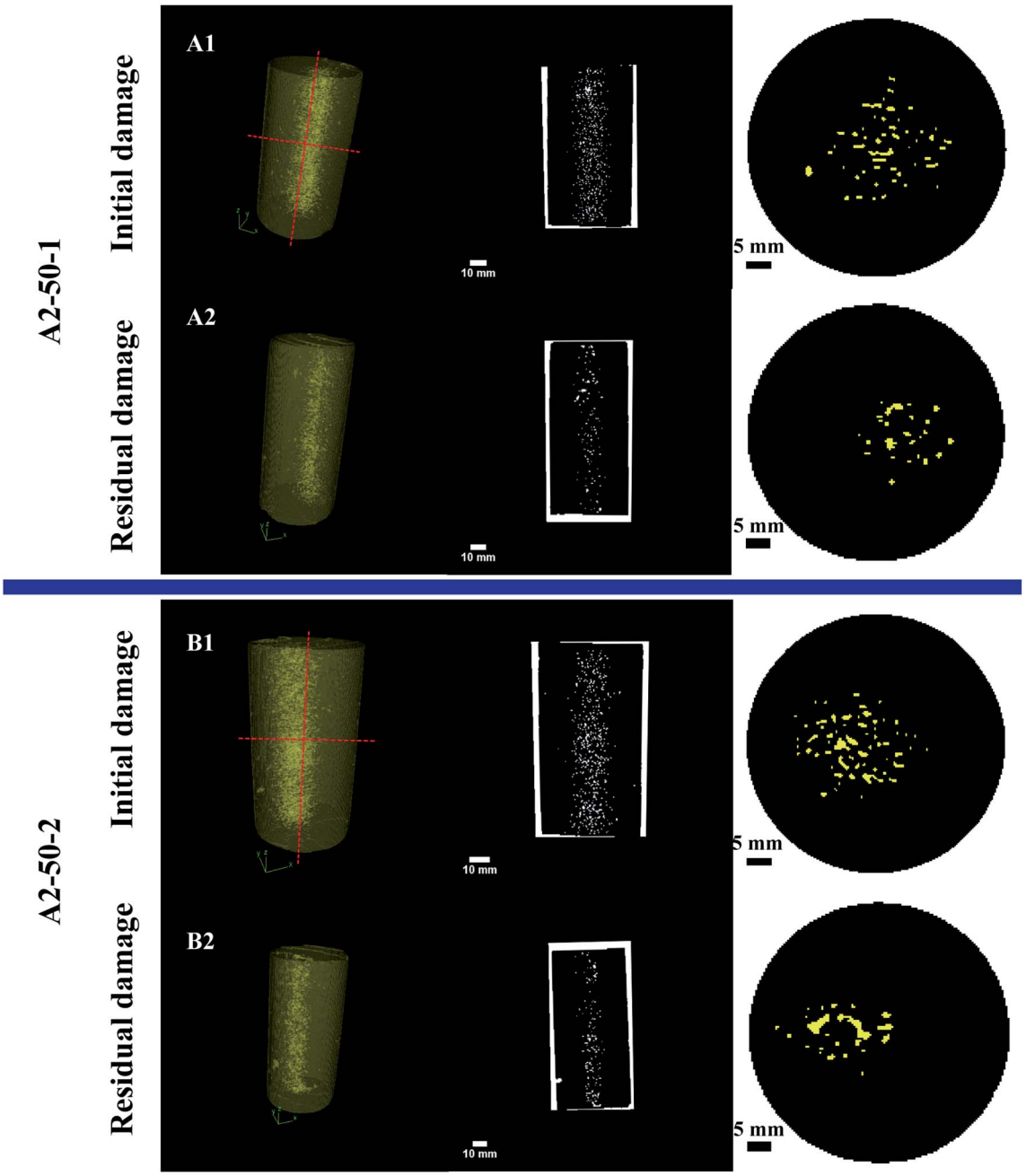

Fig. 6 3D view of salt samples reconstructed from CT slices showing the initial (A1 and B1) and residual (A2 and B2) damage. Cross sections are shown in horizontal and vertical directions at the middle part of specimen. The yellow patches indicate damage region which were used to calculate healing effectiveness.

The crystal surface was no longer smooth exhibiting shear steps. These microscopic characteristics resulted from the impact of cataclasis under high strain rates.[39] The abundant defective structures pointing to locally high strain zones are favorable for nucleation of recrystallization.[29] After healing with brine solution, the grain surface became smoother. Micro-cracks and voids significantly reduced. Most of them were healed except some large cracks (Fig. 7c), while in the case of, only a small portion of the microstructures was healed. As indicated in Fig. 7d, there were many micro-tunnels and pits left on the grain surface indicating that oil could hinder the healing process by restraining grain recrystallization in agreement with CT results. What's more, the high-resolution SEM images of them clearly depicted the differences between the grain boundary structure of brine and oil soaked specimens (Fig. 8). The amplified SEM image of brine infiltrated sample showed well-healed grain boundaries (Fig. 8b). Well contact healed structure at grain boundaries and grain boundary spacing with a small thickness (<100 nm) indicated the existence of fluids.[29] The ghost grain boundary (indicated by the red dash line)

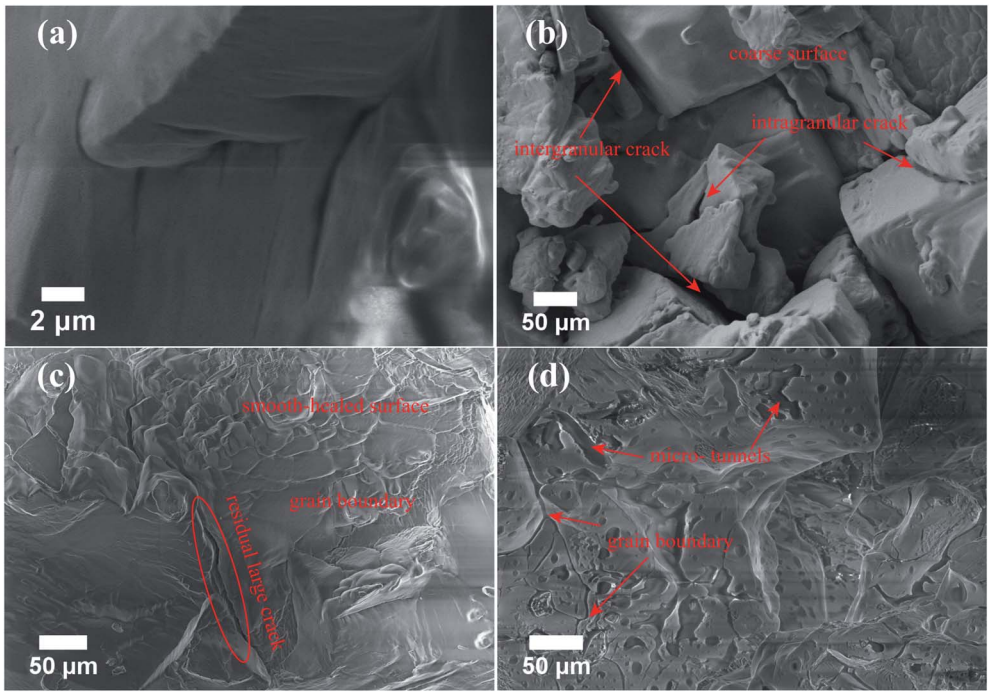

Fig. 7 SEM images of (a) original salt, (b) damaged salt, (c) damaged salt after healing with brine (A2-50-1) and (d) after healing with oil (A2-50-2).

indicated the existence of fluid film-assisted dynamic recrystallization. Due to the limits of the SEM resolution, we did not get SEM images of higher resolution to see the details of the grain boundaries internal structure. In comparison, the amplified SEM image of oil infiltrated sample displayed that there was still a relatively large spacing between two grains (Fig. 8d). Results suggested that the healing effect should be carefully considered when using salt caverns for petroleum reserve. Damage-healing constitutive models, such as the well-known MDCF model,[40,41] might need to be refined accordingly.

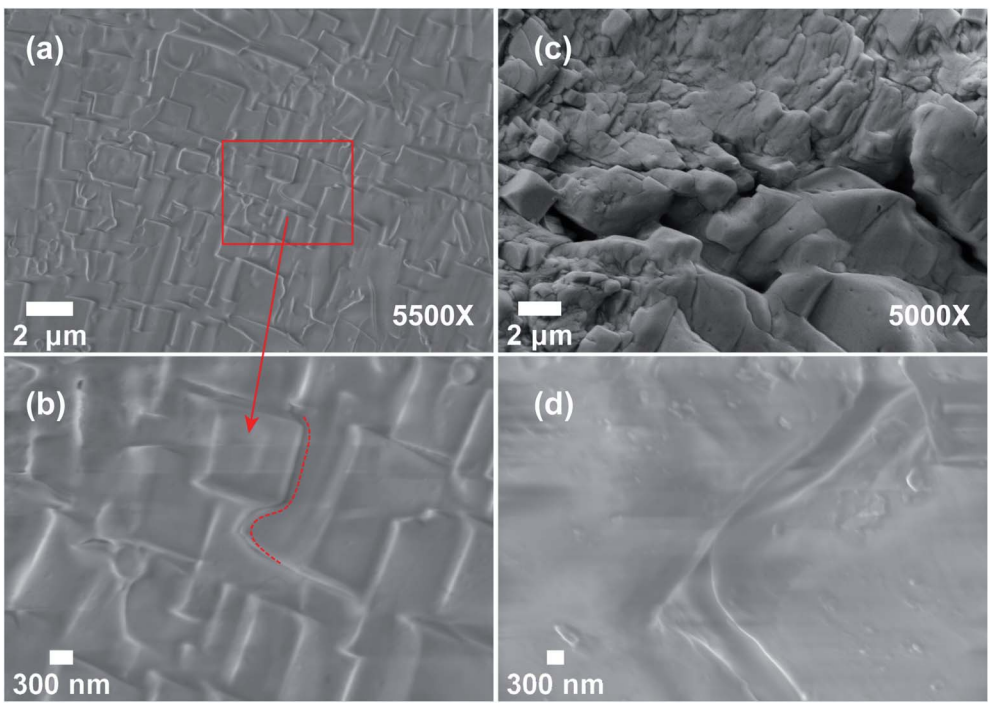

Fig. 8 High-resolution SEM images of sample A2-50-1 (a and b) and A2-50-2 (c and d), showing the differences of the grain boundary structure of brine and oil infiltrated samples. The magnifications of (a)–(d) are 5500×, 18 500×, 5000× and 13 100×, respectively.

3.4 NMR

Furthermore, to investigate the pore characteristics of rocksalt after healed, NMR was carried out. The results are shown in Fig. 9. For the relaxation mechanism of fluid-saturated pores, the transverse relaxation rate $1/T_2$ is mainly attributed to the interactions between the nuclear spin and solid surfaces in the fast diffusion limits implying a volumetric description. Generally, the transverse relaxation rate in rock samples is determined by the following equations:[42–44]

$$\frac{1}{T_2} = \frac{1}{T_{2B}} + \frac{1}{T_{2S}} + \frac{1}{T_{2D}} \quad (2)$$

where T_2 is the transverse relaxation time (ms), T_{2B} is the bulk relaxation time (ms), T_{2S} is the surface relaxation time (ms) and T_{2D} is the diffuse relaxation time (ms).

In eqn (2), T_{2S} and T_{2D} are calculated by eqn. (3) & (4):

$$\frac{1}{T_{2S}} = \rho_2 \left(\frac{S}{V}\right)_{pore} \quad (3)$$

where ρ_2 is the surface relaxivity (m ms^{-1}). $\frac{S}{V}$ is the surface-to-volume ratio of pore (m^{-1}).

$$\frac{1}{T_{2D}} = \frac{(\gamma G T_E)^2}{12} D \quad (4)$$

where γ is the gyromagnetic ratio (rad s^{-1} T^{-1}), G is the magnetic field gradient (Gs cm^{-1}), T_E is the echo spacing (ms) and D is the diffusivity (cm^2 ms^{-1}).

In general, $T_2 \ll T_{2B}$, therefore, the first item of eqn 2 can be ignored. In a homogeneous magnetic field, $1/T_{2D} \approx 0$. As a result, the transverse relaxation rate can be described as:

$$\frac{1}{T_2} \approx \frac{1}{T_{2S}} = \rho_2 \left(\frac{S}{V}\right)_{pore} = F_s \frac{\rho_2}{r} \quad (5)$$

Here, r is the pore diameter (m). Factor F_s depends on the geometric shape of pores (3 for spherical and 2 for cylindrical pores).

Eqn 5 describes the relationship between the transverse relaxation time and the pore diameter. Therefore, we could obtain pore size distribution (Fig. 9b) according to T_2 distribution (Fig. 9a). As shown in Fig. 9a, both T_2 distribution spectrums exhibited one large peak and two small peaks revealing the continuity of the pore size variation. T_2 of healed samples with brine ranged from 0.01 to 3072 ms, whereas T_2 of healed samples with oil ranged from 0.01 to 841 ms. Accordingly, r of healed samples with brine mainly ranged from 1.9 to 85.0 μm, while r of healed samples with oil mainly ranged from 0.1 to 3.3 μm. The results indicated that healed salt with the brine solution mostly consisted of macropores (>1 μm) with very little mesopores (0.1–1 μm) and micropores (<0.01 μm), however healed salt with oil mainly consisted of macro- and meso-pores with very little micropores. Herein, macropore, mesopore and micropore are defined according to pore diameter: macropore (>1 μm), mesopore (0.1–1 μm), micropore (<0.1 μm).[45] Micropores were well healed in agreement with SEM results. As we can see from Fig. 9c–e, for healed salt with brine the pore throat

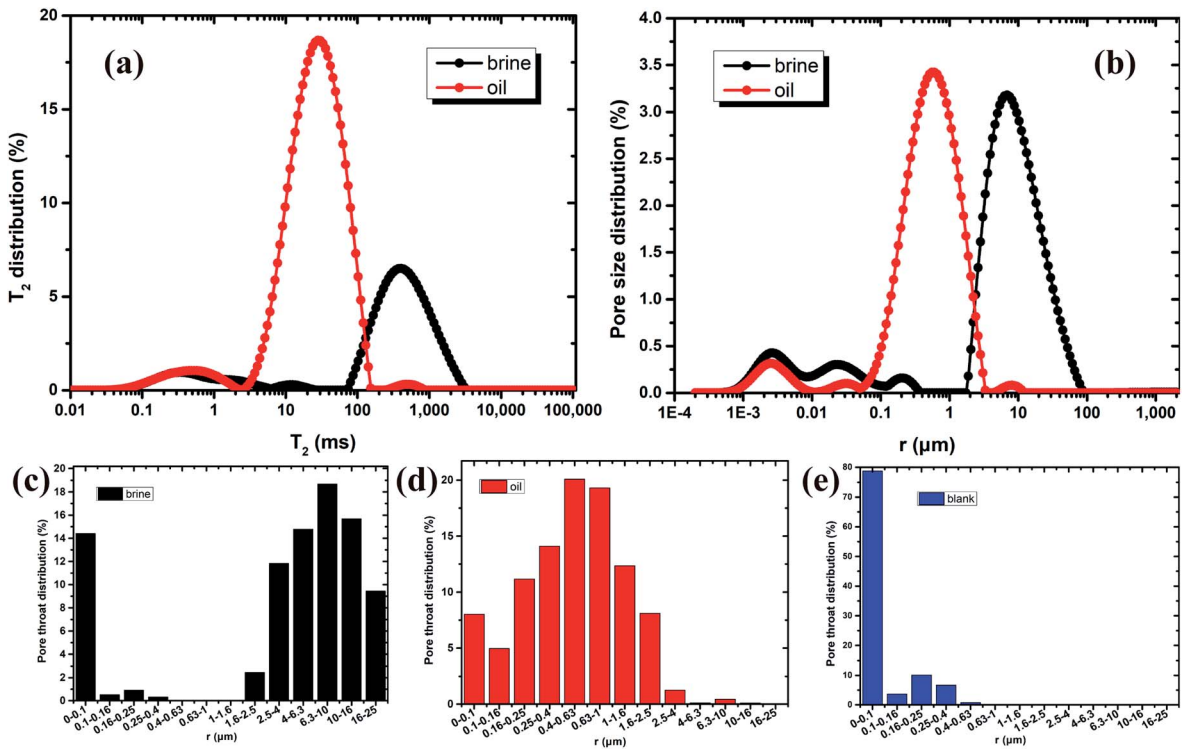

Fig. 9 Results of NMR: comparisons of (a) relaxation time, T_2 distribution and (b) pore size distribution after healing with brine and oil. Pore throat distribution of healed salt with (c) brine (A2-50-1) and (d) oil (A2-50-2). (e) Blank (A2-50-3) without brine and oil is for comparison.

Table 3 Nuclear magnetic resonance (NMR) test results: porosity, permeability and total peak area[a]

Samples no.	Healing conditions	Healing time/d	Porosity/%	Permeability/ mD*	Total peak area/ms
A2-50-1	Brine	7	0.55	0.0044	209.02
A2-50-2	Oil	7	1.24	0.0808	531.03
A2-50-3#	—	0	—	—	—

[a] #Because there was no fluid inside sample A2-50-3, we could not get valid data from NMR. *1 mD = 10^{-15} m^2.

greater than 1.6 μm accounted for 72.9%. For healed salt with oil, the pore throat less than 1.6 μm accounted for 98.1%. It also agreed with pore size analysis. Please note that the blank group (sample A2-50-3) without fluid was only for comparison. Because there was no enough fluid inside rocksalt, we could not get valid data from NMR. What's more, porosity and permeability were also obtained from NMR (Table 3). It was shown that the porosity and permeability of samples A2-50-1 were very low and less than samples A2-50-2, indicating that the healing effect could decrease the porosity and permeability of damaged rocksalt.

3.5 Discussion

Micro-damage (microcracks & microvoids) in damaged salt can be gradually recovered in suitable environments giving rise to recovery of mechanical and penetrative properties,[16,41,46]. It is an important characteristic for the operation of salt caverns since crack healing in salt will play a key role in determining the evolution of permeability and mechanics in the excavation damaged or disturbed zones (EDZ) in rocksalt repositories, particularly in long term operations.[27] Studies show that most of the healing occurs rapidly compared to the time scale over which mining or storage in salt occurs.[20,47] Healing of fluid-assisted grain boundary is driven by compaction creep and interfacial-energy-driven processes like diffusive mass transfer and recrystallization. The effect of water is prominent. Experiments confirm that without water grain boundaries of sodium chloride are essentially immobile at temperatures below 400 °C.[29]

According to the above analysis results, we could interpret that the brine solution facilitated grain recrystallization and the diffusion effect, and also provided materials for recrystallization. On the contrary, when the oil included in cracks or pores it could hinder the healing process by impeding the diffusion effect or restraining recrystallization. However, due to the restrictions on the experimental conditions in this article, there must be deficiencies and demands for further research. For instance, grain size and temperature are not considered in this paper. More evidences are required to clarify the micro-healing processes of damaged rock salt.

Healing is a common phenomenon in natural wet salts at sufficiently low intergranular effective stress. The activation energy for recovery is as low as 10.5 kJ mol^{-1}.[20] However, in many studies the effects are often neglected and they are not usually included in engineering descriptions of salt rheology, which must lead to errors in the prediction of long-term flow.

4. Conclusions

As one of the ideal energy storage systems, salt cavern storage has become a popular research topic in China due to the SPR. Many oil storage facilities are planned to be constructed in bedded salt formations in China. The first site for China's SPR salt caverns may be located in the Jintan Salt Mine, China. In summary, this paper studied a key engineering issue—damage-healing—from the microscopic scale when salt caverns are used as reservoirs. Damaged rocksalt samples were prepared by uniaxial compression tests and then healed in a saturated brine solution and oil at 50 °C for seven days. Microscopic investigations were performed with CT, SEM and NMR to study the change of rocksalt microstructures during the damage and healing processes. Results showed that microcracks could be well healed with fluids. Healing effectiveness with the brine solution was higher than that with oil. Water played an important role in healing mainly because of crystal recrystallization. Nevertheless, when included in cracks or pores oil could hinder the healing by impeding the diffusion effect and restraining recrystallization. Finally, two possible micro-healing mechanisms were discussed. The findings indicate that the healing effect plays an important role in the evolution of porosity, permeability and mechanics of the surrounding rocks, which is required to be carefully considered in engineering descriptions of salt rheology, especially in the prediction of long-term flow when salt caverns are used for energy storage.

Conflicts of interest

The authors declare no conflict of interest.

Acknowledgements

This work was supported by the National Natural Science Fund (No. 51834003, 51604044), Chongqing Postdoctoral Innovation Program (CQBX201805), Chongqing science and technology commission (No. cstc2015jcyjA90011), which are all greatly appreciated. The authors also acknowledge Dr William N. Tiedeu for English language polishing.

References

1 W. Qiao and Z. Yang, *Energy*, 2020, **193**, 116704.
2 J. Fan, H. Xie, J. Chen, D. Jiang, C. Li, W. N. Tiedeu and J. Ambre, *Appl. Energy*, 2020, **258**, 114007.
3 CNPC, *Development report of oil and gas industry at home and abroad*, 2018, http://energy.people.com.
4 X. Shi, W. Liu, J. Chen, C. Yang, Y. Li, H. Ma, H. Peng, T. Wang and X. Ma, *Adv. Mater. Sci. Eng.*, 2017, **2017**, 1–11.
5 H. Ibrahim, A. Ilinca and J. Perron, *Renewable Sustainable Energy Rev.*, 2008, **12**, 1221–1250.

6 T. M. I. Mahlia, T. J. Saktisahdan, A. Jannifar, M. H. Hasan and H. S. C. Matseelar, *Renewable Sustainable Energy Rev.*, 2014, **33**, 532–545.
7 Y. He, D. Jiang, J. Chen, R. Liu, J. Fan and X. Jiang, *Rock Mech. Rock Eng.*, 2019, **52**, 2471–2479.
8 J. L. Li, Y. Tang, X. L. Shi, W. J. Xu and C. H. Yang, *Appl. Energy*, 2019, **255**, 113866–113875.
9 W. Liu, N. Muhammad, J. Chen, C. J. Spiers, C. J. Peach, D. Jiang and Y. Li, *J. Nat. Gas Sci. Eng.*, 2016, **35**, 468–482.
10 W. Liu, J. Chen, D. Jiang, X. Shi, Y. Li, J. J. K. Daemen and C. Yang, *Appl. Energy*, 2016, **178**, 703–720.
11 W. Liu, Y. Li, C. Yang, J. J. K. Daemen, Y. Yang and G. Zhang, *Eng. Geol.*, 2015, **193**, 212–223.
12 J. Chen, D. Lu, W. Liu, J. Fan, D. Jiang and L. Yi, *J. Energy Storage*, 2020, **27**, 101131.
13 W. Liu, Z. Zhang, J. Chen, J. Fan, D. Jiang and J. Daemen, *Energy*, 2019, 682–694.
14 J. Fan, J. Chen, D. Jiang, A. Chemenda, J. Chen and J. Ambre, *Int. J. Fatigue*, 2017, **94**, 140–144.
15 F. Wu, J. Chen and Q. Zou, *Int. J. Damage Mech.*, 2019, **28**, 758–771.
16 T. Pfeifle and L. Hurtado, *Int. J. Rock Mech. Min. Sci.*, 1998, **35**, 637–638.
17 K. S. Chan, S. R. Bodner and D. E. Munson, *Int. J. Damage Mech.*, 2001, **10**, 347–375.
18 K. Fuenkajorn and D. Phueakphum, *Bull. Eng. Geol. Environ.*, 2011, **70**, 665–672.
19 J. Chen, S. Ren, C. Yang, D. Jiang and L. Li, *Materials*, 2013, **6**, 3438–3450.
20 N. S. Brodsky, *Thermomechanical damage recovery parameters for rocksalt from the Waste Isolation Pilot Plant*, Sandia National Laboratories, Albuquerque, New Mexico, 1995.
21 K. Fuenkajorn, *Suranaree J. Sci. Technol.*, 2006, **13**, 307–316.
22 L. H. Chao, M. L. Wang and S. Miao, *Microsc. Res. Tech.*, 1993, **25**, 456–464.
23 H. H. Stephen and E. Brian, *Int. Geophys.*, 1992, **51**, 253–280.
24 S. d. Meer, C. J. Spiers and S. Nakashima, *Earth Planet. Sci. Lett.*, 2005, **232**, 403–414.
25 F. Renard, J. P. Gratier and B. Jamtveit, *J. Struct. Geol.*, 2000, **22**, 1395–1407.
26 R. V. Noort, H. J. M. Visser and C. J. Spiers, *J. Geophys. Res.: Solid Earth*, 2008, **113**, 1–15.
27 M. E. Houben, A. ten Hove, C. J. Peach and C. J. Spiers, *Phys. Chem. Earth*, 2013, **64**, 95–104.
28 M. K. Darabi, R. K. Abu Al-Rub and D. N. Little, *Int. J. Solids Struct.*, 2012, **49**, 492–513.
29 O. Schenk and J. L. Urai, *Contrib. Mineral. Petrol.*, 2004, **146**, 671–682.
30 P. M. T. M. Schutjens and C. J. Spiers, *Oil Gas Sci. Technol.*, 1999, **54**, 729–750.
31 J. Fan, J. Chen, D. Jiang, S. Ren and J. Wu, *Int. J. Fatigue*, 2016, **90**, 109–115.
32 C. E. Fairhurst and J. A. Hudson, *Int. J. Rock Mech. Min. Sci.*, 1999, **36**, 279–289.
33 J. Fan, D. Jiang, W. Liu, F. Wu, J. Chen and J. J. K. Daemen, *Int. J. Rock Mech. Min. Sci.*, 2019, **115**, 77–86.
34 D. Jiang, J. Fan, J. Chen, L. Li and Y. Cui, *Int. J. Rock Mech. Min. Sci.*, 2016, **86**, 255–260.
35 N. Thiemeyer, J. Habersetzer, M. Peinl, G. Zulauf and J. Hammer, *J. Struct. Geol.*, 2015, **77**, 92–106.
36 J. Schmatz, J. Klaver, M. Jiang and J. L. Urai, presented in part at the *SPE Bergen One Day Seminar*, Bergen, Norway, 2017.
37 M. Hamami, *Geotech. Geol. Eng.*, 2006, **24**, 1271–1292.
38 J. L. Urai, C. J. Spiers, H. J. Zwart and G. S. Lister, *Nature*, 1986, **324**, 554–557.
39 C. W. Passchier and R. A. J. Trouw, *Microtectonics*, Springer Berlin Heidelberg, 2005.
40 K. S. Chan, S. R. Bodner, A. F. Fossum and D. E. Munson, *Constitutive representation of damage development and healing in WIPP salt*, American Rock Mechanics Association, 1995, vol. 10, pp. 623–642.
41 K. S. Chan, S. R. Bodner and D. E. Munson, *Int. J. Damage Mech.*, 1998, **7**, 143–166.
42 M. Fleury and M. Romero-Sarmiento, *J. Pet. Sci. Eng.*, 2016, **137**, 55–62.
43 H. Liu, M. Nogueira d'Eurydice, S. Obruchkov and P. Galvosas, *J. Magn. Reson.*, 2014, **246**, 110–118.
44 S. Wiete, G. Hans-Reinhard, M. Ivonne and S. Frank, *J. Appl. Geophys.*, 2008, **65**, 21–29.
45 B. B. Ходот, *Coal and Gas Outburst*, China industry press, Beijing, 1966.
46 L. M. Kachanov, *Izv. Akad. Nauk SSSR, Otd. Tekh. Nauk*, 1958, **8**, 26–31.
47 L. S. Costin and W. R. Wawersik, *Creep healing of fractures in rock salt*, Sandia National Laboratories, 1980, pp. 1–33, SAND80-0392.

